Hindawi
Advances in Civil Engineering
Volume 2020, Article ID 8881800, 13 pages
https://doi.org/10.1155/2020/8881800

Research Article

Ultrasonic Spectrum Analysis of Granite Damage Evolution Based on Dry-Coupled Ultrasonic Monitoring Technology

Yang Liu,[1] **Lan Qiao**,[1] **Yuan Li**,[1] **Guodong Ma**,[1] **and Andrei M. Golosov**[2]

[1]*Department of Civil Engineering, University of Science and Technology Beijing, Beijing 100083, China*
[2]*School of Engineering, Far Eastern Federal University, Vladivostok 690091, Russia*

Correspondence should be addressed to Yuan Li; liyuan@ustb.edu.cn

Received 16 June 2020; Revised 19 August 2020; Accepted 3 September 2020; Published 29 September 2020

Academic Editor: Fengqiang Gong

The self-developed dry-coupled rock ultrasonic monitoring system is adopted to set up a multidirectional and multiwaveform ultrasonic monitoring network, which aims to analyse the evolution law of acoustic spectrum parameters in the process of granite loading failure under uniaxial compression, to explore the dominant acoustic spectrum characteristic information at different stages of granite loading, and to verify in situ the damage monitoring of time-effect deformation. The results show that the wave velocity, amplitude, and amplitude-frequency of the first wave and the velocity of P-wave and S-wave show a significant upward trend in the rock compaction section. After entering the elastic stage, the three spectral parameters become peacefully stable, and the stage transformation is obvious. In the stable crack growth stage, with the initiation of the crack, the dominant frequency of S-wave shows a significant stage transition compared with the global ultrasonic wave velocity and the first arrived amplitude, and the dominant frequency decreases by 6%. In the unstable crack growth stage, the three acoustic spectrum parameters present obvious downward trend, and the first arrived wave amplitude of S-wave is found to have a significant decline of 39.1%. On the eve of failure, the amplitude-frequency of S-wave shows different feature from the P-wave; that is, S-wave transfers from the state of multipeak in wide frequency to the state of single peak in low frequency, which is the failure precursor of the rock sample.

1. Introduction

With the advancement of geotechnical engineering to the depth, underground engineering faces complex conditions such as high stress. The complex rock mechanical response such as spalling [1, 2] and rockburst [3, 4] is accompanied by the excavation process. Therefore, it is of great significance to study the law of rock damage evolution and damage prediction for the prevention and control of deep engineering disasters. At present, the theory and numerical simulation of rock mechanics are not complete [5]. Rock mechanics test, as an important method to study rock mechanics problems, can strictly control environmental conditions, analyze and solve rock mechanics problems more accurately, and provide data and theoretical basis for solving engineering safety problems.

The propagation characteristics of sound wave in rock are closely related to the elastic property of rock. Different from the strain gauge, it can only monitor the local surface deformation; sound wave inherits good penetrability inside many mediums including rocks. The evolution of fractures in the whole rock can be well characterized; this can be seen by the changes of wave velocity [6] and amplitude-frequency [7]. The energy characteristics of acoustic emission are related to the mode of crack coalescence, which can effectively characterize the generation and development of cracks and the failure of rock [8]. Jianpo et al. used acoustic emission (AE) technology to monitor the gradual fracture development around the tunnel surrounding rock under the static stress and dynamic disturbance; the power-law characteristics of AE signals after blasts can be used to evaluate the time required for rock mass to return to a stable state [9]. GuiLin et al. studied the relationship between maximum AE energy and the number of defects in prefabricated rocks through uniaxial loading tests of prefabricated fractured rocks [10]. Xiao et al. showed that AE parameters could

effectively characterize the critical stage of rock damage and the maximum critical threshold of freeze-thaw cycle times resulting in rock damage based on a large number of freeze-thaw cycle rock tests [11].

As a nondestructive testing method, ultrasonic testing can be used to set the superiority ultrasonic source frequency and the source pulse amplitude, which is less affected by environmental noise, compared with the single function that acoustic emission can only receive elastic waves [12, 13]. At present, rock damage based on ultrasonic wave has been studied to some extent. Falls and Young carried out a deep granite tunnel damage study based on ultrasonic wave velocity [14]. Based on the similar theory, Dong et al. obtained the ultrasonic speed-stress relationship of Jinping-II Hydropower Stations diversion tunnel [15]. Shili et al. thought that the wall-rock velocity adjacent to the surface of underground openings is a vital support design parameter [16]. Multiparameter relationships occurred among ultrasonic velocities with seismic fracture and fissure indexes and physical and mechanical properties of the rock [17]. Heidari et al. evaluated the velocity of P- and S-waves and the return energy of these waves at different axial and lateral stresses on a rock specimen in order to determine the dynamic mechanical parameters of rocks [18]. Nascimento et al. explored the relationship between elastic wave velocity and fracture density [19]. McCan and Sothcott studied the P-wave velocity, S-wave velocity, and attenuation characteristics of sandstone and limestone with a certain frequency of ultrasonic wave and obtained the attenuation and absorption mechanism of rock to sound waves [20]. Confining pressure, crack angle, and the number of cracks all have a certain influence on the velocity and attenuation of elastic waves [21]. Engelder and Plumb studied the relationship between the strain relaxation characteristics and the ultrasonic properties of rock [22]. Quan et al. conducted a regression analysis of rock damage factor determined by wave velocity and obtained the rock damage evolution equation with time [23]. However, a single wave velocity measurement leaves out a lot of important information. The complex pore structure can significantly affect the dispersion properties of elastic wave [24].

At present, researches on rock damage based on ultrasonic waves mostly focus on the analysis of rock acoustic spectrum characteristics with a single direction and a single waveform, but lack the analysis of rock acoustic spectrum characteristics with multiple directions and waveforms, so as to select the optimal acoustic spectrum characteristics to define the degree of rock damage. At the same time, the traditional large-size ultrasonic planar sensors are unable to be applied to the multicurvature rock surface, and the use of coupled agent cannot realize the stable transmission of monitoring signal. Based on the self-developed dry-coupled small-size ultrasonic monitoring technology, this paper explored the acoustic spectral characteristics of the whole process of rock damage evolution in multiple directions and multiwaveform, which provided a method and basis for the damage discrimination of tunnel in site.

2. Study on the Ultrasonic Spectral Characteristics in Multiposition and Multiparameter during Uniaxial Loading of Granite

Based on the problems mentioned above, it is urgent to realize the comprehensive long-term core damage monitoring of core release on-site. The liquid-coupled agent of traditional coupled probe has poor durability and is easy to leak or overflow from the sensor. The coupled agent with high viscosity is not stable for the S-wave test signal [25], which is easy to cause signal loss. Furthermore, the traditional large-size planar probe cannot adapt to a variety of curvature test surfaces. The essence of dry-coupled is that the size of the acoustic contact zone of oscillating probe surface with the surface of the test object is many times smaller than the length of the ultrasound wave. Compared to the wavelength, the contact with the size of the zone less than 2 mm can be considered as point contact. In this case, the contact liquid makes no influence on the coefficient of signal transformation and became useless. The transducer acts on the test object surface as a point oscillating force [26]. Based on the dry-coupled ultrasonic monitoring system developed by the research group, this paper carried out the acoustic spectrum analysis of the laboratory test of rock samples, providing guidance for the selection of the core damage index of dry-coupled ultrasonic monitoring and the definition of the rock damage evolution stage.

2.1. Test System and Sample Preparation. Ultrasonic monitoring using self-developed dry-coupled acoustic technology based on rock damage monitoring system has already calibrated according to relevant reference and stipulation [27]. The monitoring system mainly includes small-size dry-coupled point contact acoustic generator and the receiving probe. This system can work without the coupled agent and is suitable for a variety of curvatures of working face; what is more, the system can be embedded in rock drilling. The system has a digital multifunctional integrated circuit board (see Figure 1) which controls the transmission pulse and ultrasonic frequency conversion in real time. The system can be used with PC machine to implement the arrangement of a three-dimensional multireceiver ultrasonic monitoring network for rocks of various sizes and curvature. The emission frequency range is 50–260 kHz, and the receiving waveform has a maximum sampling rate of 1GSa/s and a maximum acquisition frequency of 1Hz. The test loading system adopts Chaoyang TAW2000 machine. The schematic diagram of the experimental mechanical loading and acoustic monitoring system in this paper is shown in Figure 2.

In this paper, the granite was taken from Sanshan Island Gold Mine in Shandong Province at −795 m; selected granite samples inherited a relatively small anisotropic wave velocity to reduce the influence of the material itself on the data dispersion. 5 standard rock samples were processed as $\varphi 50 \times 100$ mm, and the parallelism and perpendicularity met the ISRM requirements, which is shown in Figure 3.

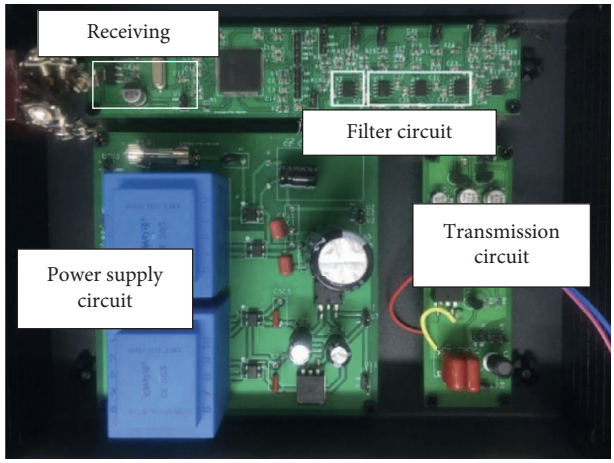

Figure 1: Digital multifunctional integrated circuit board.

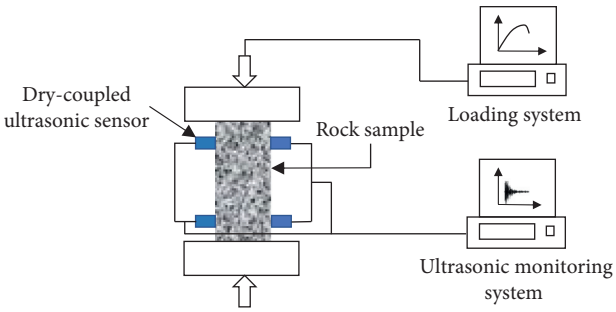

Figure 2: Schematic diagram of mechanical loading and ultrasonic monitoring system.

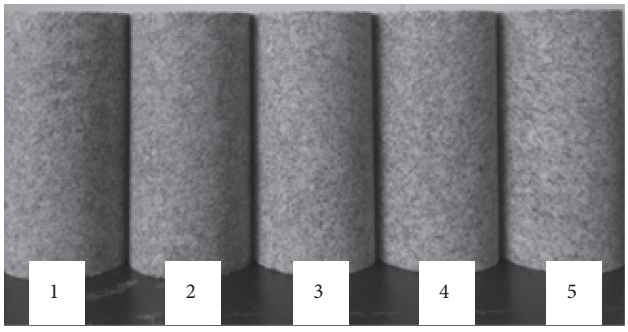

Figure 3: Granite samples.

2.2. Experimental Method. The unpredictability of the propagation path of ultrasonic wave is caused by the unbalance of the fracture initiation location and the uneven development degree during the loading process. The problem of misjudging the damaged area position based on ultrasonic wave exists in the layout of multitransmitting and multireceiving probes. In this paper, the ultrasonic probe layout scheme of single transmitter with multiposition receivers is adopted. As shown in Figure 4, the ultrasonic source sensor is arranged at the position of CH1 at the rock sample, and the ultrasonic receiving sensor is arranged at the positions of CH2, CH3, and CH4. The essence of the pulse emitted by the acoustic probe is the conversion of the electrical signal to the mechanical vibration signal, namely, the inverse piezoelectric effect, and the receiving probe works the other way around. The CH1 for ultrasonic source sensor, due to the piezoelectric ceramic in the condition of incentive, to point load on the test surface is equivalent to applying the method; the longitudinal wave and S-wave are inspired [28]. The vibration direction of the particle caused by the S-wave is perpendicular to the surface of the rock block, which is the same as the receiving vibration direction of the receiving probe CH3 piezoelectric ceramics, so the S-wave can be received by the receiving probe CH3, which is on the same side as the transmitting probe CH1 [29]. The CH2 and CH4 probe first receives the ultrasonic wave propagating in the direction of CH1, among which only the longitudinal wave whose vibration direction is consistent with the propagation direction can cause the piezoelectric ceramics vibration of CH2 and CH4, so the CH2 and CH4 probe can receive the longitudinal wave. Therefore, in this paper, CH2 and CH4 are used as primary wave (P-wave) reception sensors, and CH3 is used as secondary wave (S-wave) sensor. Among them, CH1-CH2 is the local contralateral P-wave monitor of rock, CH1-CH4 is the overall oblique P-wave monitor of rock, and CH1-CH3 is the unilateral S-wave monitor of rock. The ultrasonic frequency is set to 125 kHz, and the automatic ultrasonic transmission and reception is realized through the control circuit. The waveform sampling rate is 25 MHz, and the sampling interval between waveforms is 2s. The loading rate is 50 N/s. The fitting condition of the dry-coupled ultrasonic wave sensor and the rock sample surface should be checked before the test.

2.3. Test Results and Analysis

2.3.1. Damage Evolution Characterized by Stress-Strain Data. The typical stress-strain curve of the deformation and failure process of the granite sample under uniaxial loading is shown in Figure 5. Due to limited space, this paper mainly focuses on the analysis of sample 1. The four typical stages of granite are distinguished by the characteristic stresses related to microcracks [30], namely, the closing stress σ_{cc}, the crack initiation stress σ_{ci}, the unstable propagation stress of the crack σ_{cd}, and the peak strength σ_f. The calculation of the total volume strain of the rock sample can be expressed as

$$\varepsilon_v = \varepsilon_1 + 2\varepsilon_3, \tag{1}$$

where ε_v is the total volumetric strains, ε_1 is the axial strain, and ε_3 is the lateral strain.

$$\varepsilon_v^{\text{cra}} = \varepsilon_v - (1 - 2\nu)\frac{\sigma}{E}, \tag{2}$$

where $\varepsilon_v^{\text{cra}}$ is the crack volumetric strains, ν is Poisson's ratio, σ is the axial stress, and E is Young's modulus.

The uniaxial loading deformation and failure process of granite sample in Figure 5 can be divided into four stages, that is, the compaction stage i, the elastic stage ii, the stable crack propagation stage iii, and the unstable crack propagation stage iv. At the compaction stage i, the axial stress ranges from 0 to σ_{cc}, the original cracks of rock close gradually, and the volume

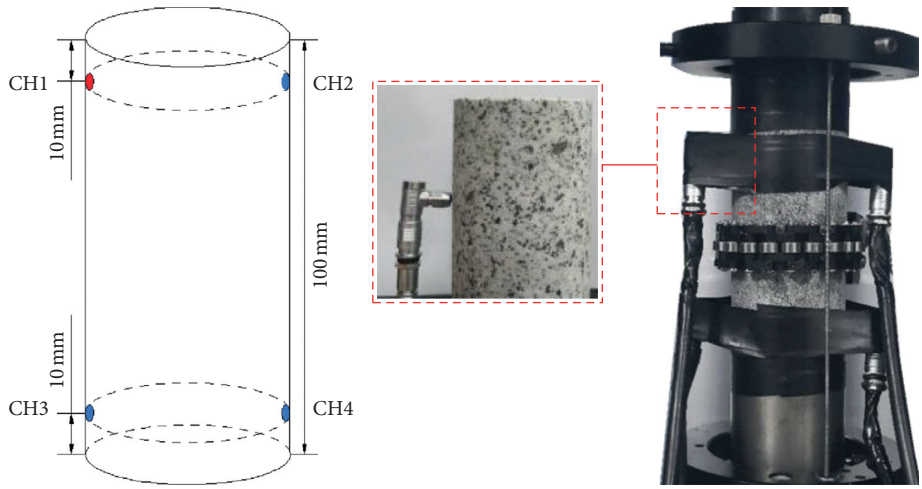

Figure 4: Arrangement scheme of the dry-coupled ultrasonic sensor.

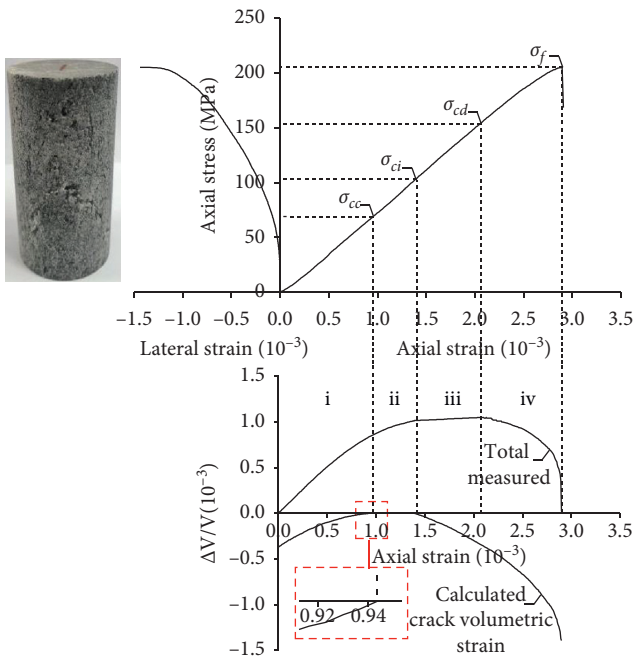

Figure 5: Stress–strain of granite under uniaxial loading.

strain of crack approaches to zero under pressure. At elastic stage ii, the axial stress ranges from σ_{cc} to σ_{ci}, and the friction generated by the closure fracture surface limits the sliding of the fracture surface, resulting in the failure of the initiation and development of new fractures; thus, the rock sample presents elastic deformation macroscopically. At the stable crack propagation stage iii, the axial stress varies from σ_{ci} to σ_{cd}, new cracks start to appear with the increase of the fracture volume, and the growth rate of the volume strain continues to decline until the reverse point corresponding to the damaging stress σ_{cd}. When entering the unstable crack propagation stage iv, the axial stress grows from σ_{cd} to σ_f; the growth rate of cracks increases significantly with the axial stress rising rapidly to the peak stress, thus leading to the failure of the rock sample.

2.3.2. Damage Evolution Characterized by the Velocity of P-Wave and S-Wave. When ultrasonic wave propagates inside the rock, the attenuation changes of P-wave and S-wave are closely related to the development of rock cracks [18]. The key to ultrasonic velocity extraction is to acquire the first wave arrival time. In this paper, wavelet denoising algorithm is used for filtering treatment. High decomposition levels in wavelet denoising can reduce the fidelity of received signals. In this paper, db8 wavelet, decomposition level of 4, Heursure rules, threshold adjustment strategy "MLN," and hard threshold algorithm are adopted to denoise the ultrasonic reception waveform. Therefore, the evolution law of the ultrasonic wave velocity in the whole process of rock failure can be obtained (see Figure 6) combined with the improved AIC algorithm of the research group [31].

Crack closure stage i: as crack closes, the P-wave velocity of CH2 and CH4 and the S-wave velocity of CH3 rise rapidly. When the axial stress arrived at σ_{cc}, the P-wave velocity of CH2, CH4, and CH3 had increased by 6.92%, 5.47%, and 4.04%, respectively, among them, CH2, as the nearest area to the press head, had the highest growth rate and became stable at the earliest, which indicated an unbalanced development of the deformation of rock under uniaxial loading.

Elastic stage ii: no crack initiation and development occurred in this stage, and the wave velocity at the three positions remained basically unchanged.

Stable crack growth stage iii: new cracks started to occur, ultrasonic wave energy tended to decline affected by scattering and reflection of ultrasonic, and the energy transmission path became longer. The P-wave velocity near the press head (CH1-CH2) reduced by 3.24%, the S-wave velocity at the unilateral surface area (CH1-CH3) dropped by 1.3%, and the P-wave velocity at the oblique area (CH1-CH4) decreased by 3.52%. In this phase, the P-wave and S-wave velocity decreased at a small rate in each region of the rock sample, and the overall transformation of wave velocity was not obvious.

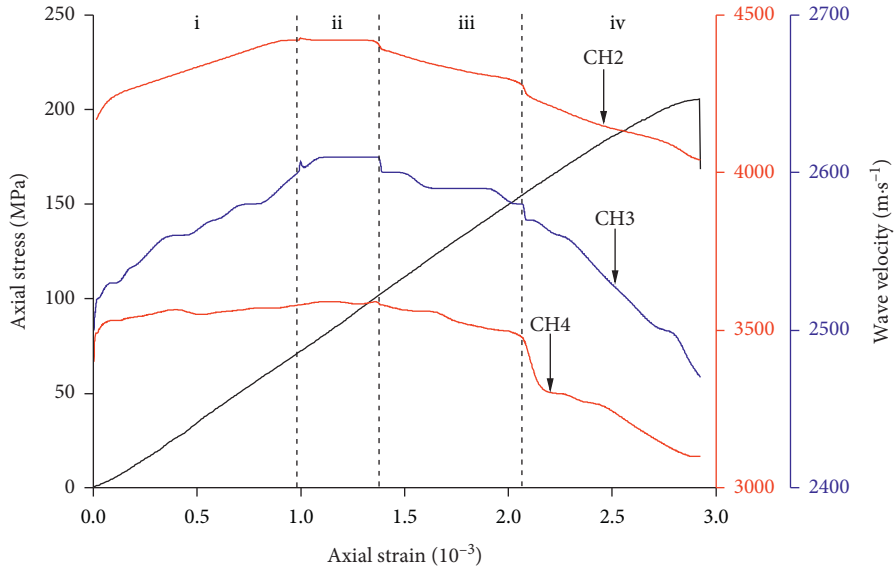

Figure 6: Ultrasonic velocity of granite at three locations under uniaxial loading.

Unstable crack growth stage: the volume strain of the crack increased rapidly and steeply, and the crack gradually expanded into a macroscopic fracture. The P-wave velocity of CH1-CH2 decreased by 5.17%, the P-wave velocity of CH1-CH3 declined by 3.83%, and the P-wave velocity of CH1-CH4 dropped by 10.37%.

In summary, the sensitivity of P-wave and S-wave to rock damage evolution is not ideal. An obvious transformation only occurs in the compaction stage and the unstable crack propagation stage; meanwhile, the S-wave decline rate is significantly higher than that of the P-wave on the eve of failure.

2.3.3. Damage Evolution Characterized by the First Arrived Wave Amplitude of P-Wave and S-Wave. Cavity, crack, and other damage inside the rock will influence the diffraction, transmission, and reflection of the ultrasonic, resulting in ultrasonic energy loss. The peak amplitude of the first wave directly reflects the attenuation degree of the ultrasonic energy in the transmission process and thereby reflects the development degree of rock damage.

The first wave amplitude of granite monitored by ultrasonic under uniaxial compression is shown in Figure 7. At the crack closure stage, loading start from 0 to σ_{cc}, the original cracks in the rock sample are compacting due to increasing load; the energy attenuation from ultrasonic continues to drop hereby as the first wave amplitude continues to rise. However, there exist differences of the amplitude rising rate among P-wave and S-wave; this is reflected by the following: (1) The first arrived P-wave amplitude of CH2 increases rapidly at the beginning in a very short time and then starts to drop; this indicates that the deformation of the rock sample near the press head is faster than the global deformation; namely, the deformation of the rock sample under uniaxial load is unbalanced. (2) The first arrived S-wave amplitude of CH3 tends to grow steadily and is lower than P-wave of CH2 and CH4 on the whole. (3). When the first arrived wave amplitude of CH4 reaches the point of σ_{cc}, the overall crack closure process of CH1-CH4 region is almost finished, which is coincided with the global compaction process. (4) The different evolution laws at different positions show that the changes of first arrived wave from multiposition can well reflect the development of the cracks during the compaction. Specifically, the transmission region of CH1-CH4 which goes through the sample obliquely presents the best performance to reflect the global compaction extend. When entering the elastic stage, the area of CH1-CH2 near the press-head tends to generate damage earlier than that of CH1-CH3 and CH1-CH4. The change rate of the amplitude at CH1-CH2 starts to decrease, and the amplitude at CH1-CH3 and CH1-CH4 tends to be stable without any cracks. At the stable crack growth stage, the frictional and scattering effects of the microfracture surface appear, and the first wave amplitude of the three channels showed a slow decreasing trend. When approaching the unstable crack growth stage, the first amplitude of the three channels drops down obviously at the beginning of this stage, and the position of the turning points is consistent with σ_{cd}. The first arrived amplitude of ultrasonic wave in CH1-CH2, CH1-CH3, and CH1-CH4 regions decreases by 18.4%, 39.1%, and 5.6%, respectively, compared with the mean amplitude of the elastic stage. Additionally, S-wave is more sensitive to rock damage than P-wave.

2.3.4. Damage Evolution Characterized by Amplitude-frequency Characteristics of P-Wave and S-Wave. Rock has a frequency selective absorption effect on sound waves [32]. For the actual continuous signals, the spectrum of the frequency domain is large after Fourier transform; however, compared with the dominant frequency of transmission, the signal energy in the overlow and overhigh frequency band is low, which can be ignored. In this paper, the dominant

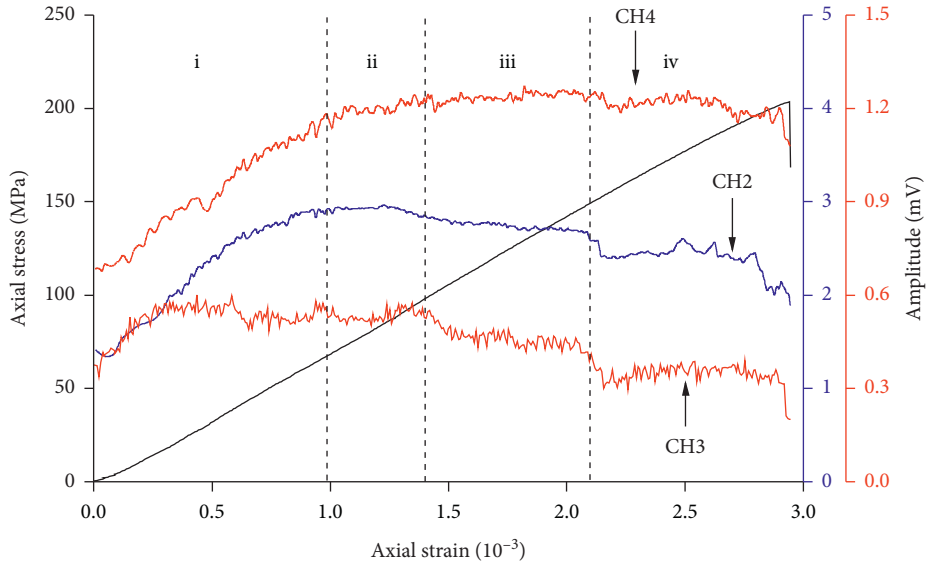

Figure 7: Amplitude of the first arrived wave of granite at three locations under uniaxial loading.

frequency of the transmitting pulse is 125 kHz. Figures 8(a)–8(c) are the curves of amplitude–frequency of channels CH2, CH3, and CH4 after rock preloading. Considering the weak energy of the high-frequency ultrasonic wave and the ultrasonic transmitting frequency parameters, the frequency band of 0–250 kHz is selected for analysis.

The amplitude-frequency characteristics in the rock loading process are often accompanied by several wave peaks with similar amplitudes. The single dominant frequency method is used to show the change of the single maximum energy frequency in the rock loading process, which cannot reflect the concentrated frequency band of the ultrasonic energy more effectively and truly. This paper introduces the centroid frequency that describes the frequency weighting characteristics in the whole frequency band range:

$$f_c = \frac{\sum_{i=0}^{N} f_i |A(f_i)| \Delta f}{\sum_{i=0}^{N} |A(f_i)| \Delta f}, \quad (3)$$

where f_c is the centroid frequency, f_i the is ultrasonic frequency, $A(f_i)$ is the amplitude corresponding to the ultrasonic frequency f_i, and Δf is the frequency increment.

The centroid frequency reflects the energy distribution of different frequency bands in the whole uniaxial loading process of rock. Figure 9 shows that CH2, CH3, and CH4 centroid frequency change and the four stages of typical amplitude-frequency characteristic in rock loaded process. Figure 9 shows the following: (1) Crack closure stage: the centroid frequency of CH2 and CH4 P-wave and CH3 S-wave is rapidly rising, showing that crack closure is more conducive to the spread of high-frequency wave; both the transmitted P-wave and S-wave exhibit multipeak amplitude-frequency characteristics, but the different frequency energy distribution of CH3 S-wave is relatively uniform. (2)The elastic stage: CH2, CH3, and CH4 centroid frequency are relatively stable, showing that the ultrasonic energy of different frequency distribution almost does not change, but the high-frequency component of CH3 S-wave is more abundant than CH2 and CH4 P-wave; S-wave centroid frequency concentrated on 115000 Hz, significantly higher than CH2 and CH4 P-wave, that are near 96000 Hz, increased by 19.8%. (3) Stable crack growth stage: the initiation of microfractures has not yet produced attenuation effect on high-frequency waves, and the amplitude-frequency characteristics of transmitted P-wave and S-wave is always in a multipeak state, but the peak values are reduced. (4) Unstable crack growth stage: the centroid frequency of P-wave and S-wave dropped rapidly and the multipeak amplitude in the amplitude-frequency also decreased significantly, indicating that the crack expansion had a significant attenuation effect on the high-frequency ultrasonic wave. CH2 and CH4 P-wave, on the eve of rock sample destruction, due to the rapid development of crack in the rock, multiple scattering, refraction, and reflection effects on the P-wave transmission, the energy attenuation of the P-wave decays significantly, resulting in the rapid attenuation of energy in the whole frequency band of the P-wave; the CH3 S-wave in the late of the unstable crack development stage, although the centroid frequency is higher, but the actual high-frequency energy has tended to have more uniform distribution of low energy, and there is only low-frequency single-peak phenomenon. Amplitude–frequency characteristics of granite no. 1–5 on the eve of failure are shown in Figure 10; for ease of expression, the amplitude has been normalized, and it indicates that there is a single low-frequency ultrasonic wave in S-wave, which is highly sensitive to rock at this stage. At the same time, the amplitude–frequency characteristics of the

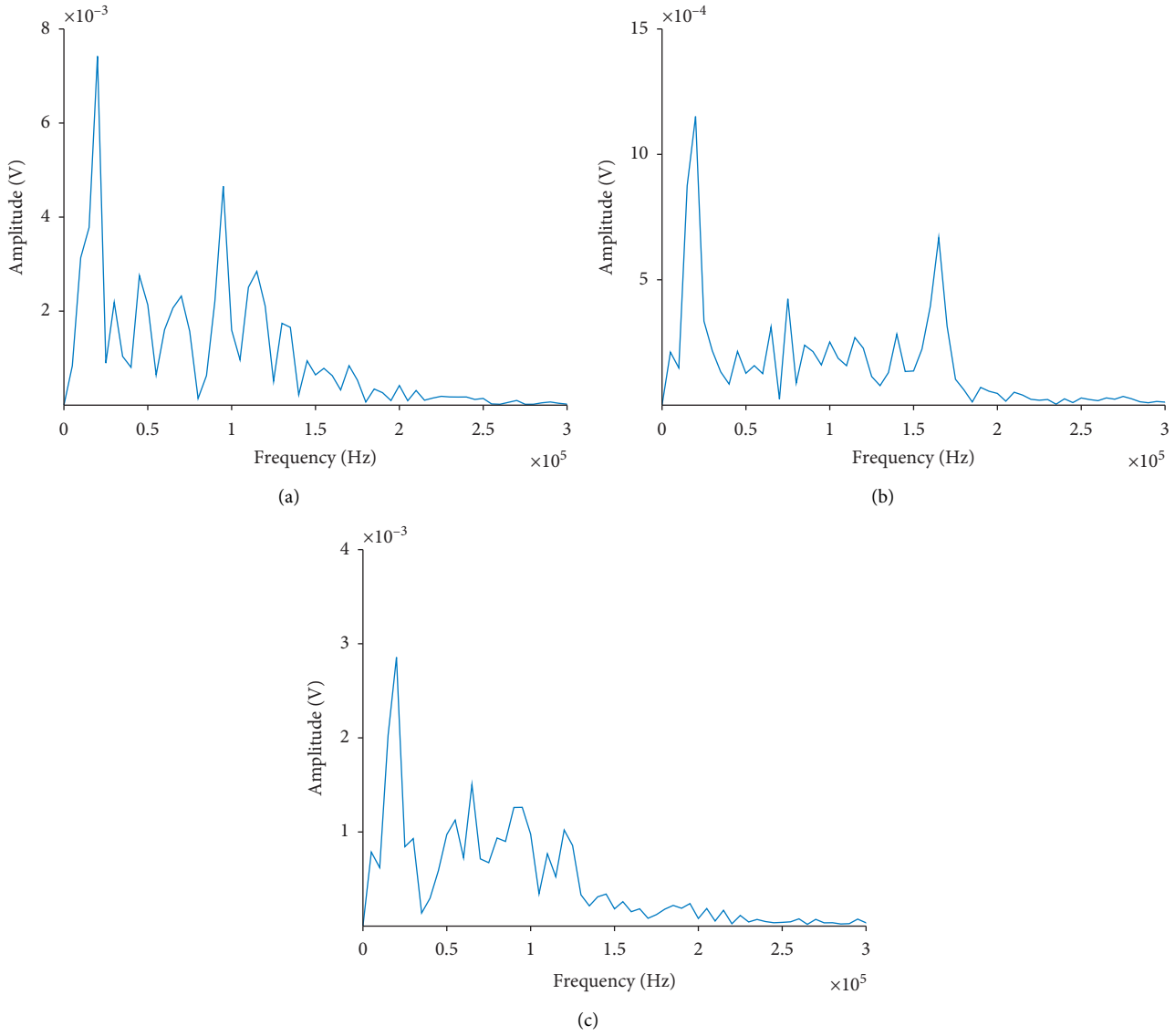

Figure 8: Amplitude–frequency characteristics of ultrasonic wave after rock preloading. (a) Amplitude-frequency characteristics of CH2. (b) Amplitude-frequency characteristics of CH3. (c) Amplitude-frequency characteristics of CH4.

S-wave before the failure of rock show the phenomenon of changing from the multipeak state in the wide band to the single-peak state in the low band, which is of great practical significance for the identification damage stage and failure prediction of the granite.

The centroid frequency and the amplitude-frequency of granite sample at crack closure stage and unstable crack growth stage showed good sensitivity, but elastic stage to stable crack growth stage shift characteristics is not obvious. Based on the above plain measurement method and the highly sensitive characteristics of S-wave damage in CH1-CH3 region, the variation law of S-wave in CH1-CH3 region during the whole loading process of rock samples was further analysed. Figure 11 shows the dominant frequency variation during the whole loading process of the granite samples. The S-wave in the CH1-CH3 region changed from the elastic phase ii to the stable crack growth stage iii; with the emergence of the crack, the dominant frequency decreased by 6%.

The above comparison of various ultrasonic wave spectrum characteristics showed that the dry-coupled ultrasonic wave level test method(CH1-CH3) only needs a single test surface for monitoring, which is suitable for the arrangement of core and borehole, and is more widely applicable to the working environment than at least two test surfaces of the opposite direction method (CH1-CH2, CH1-CH4). Besides these, in the later of the unstable crack growth stage, the amplitude-frequency characteristics of the S-wave were changed from the wide-band multipeak state to the low-band single-peak state, which provided data and technical support for the identification of damage stage and failure prediction of rock.

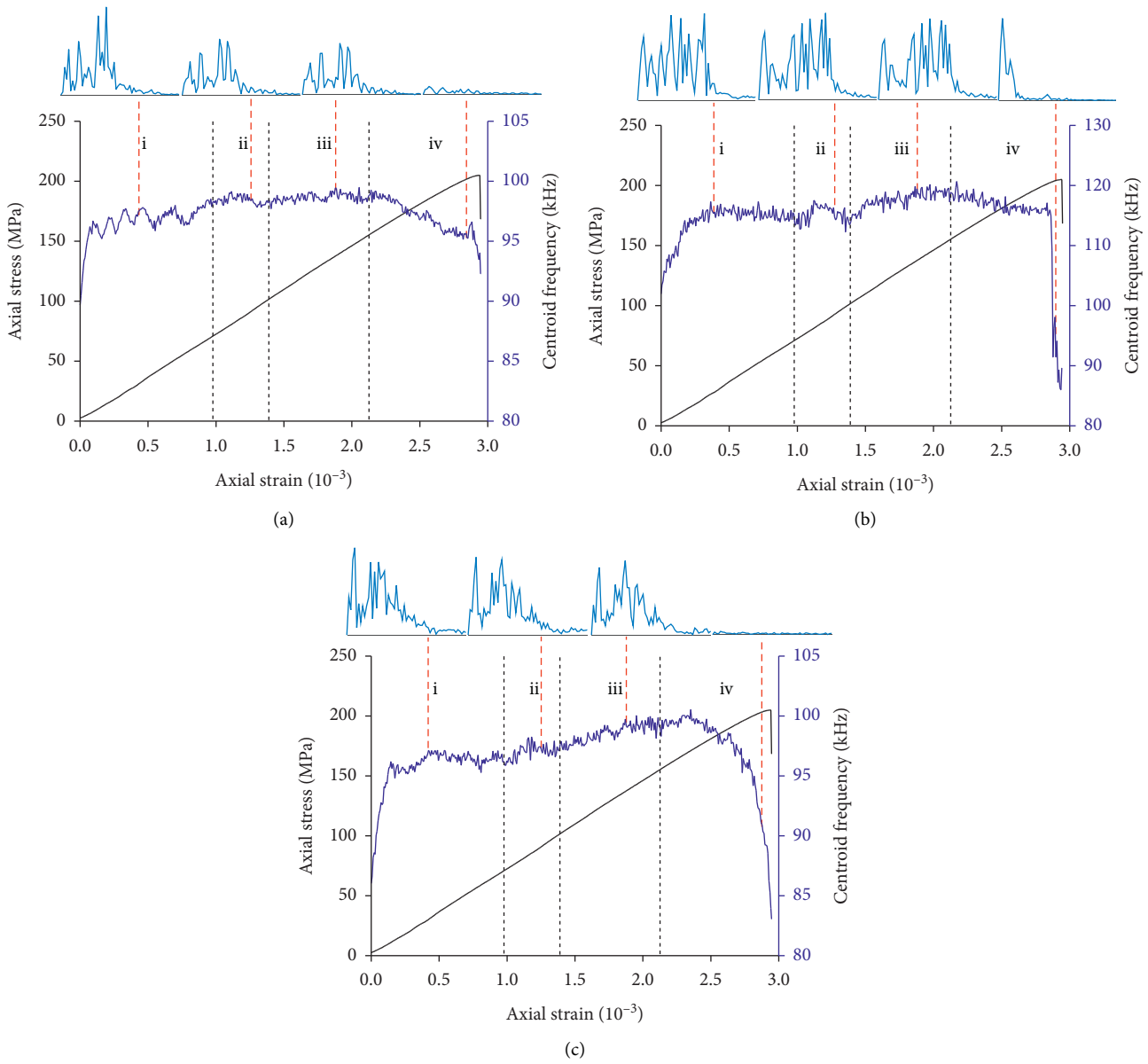

Figure 9: Centroid frequency and amplitude–frequency characteristics of granite sample at three locations under uniaxial loading: (a) CH2; (b) CH3; and (c) CH4.

3. Engineering Application

Rock deformation occurs under in situ stress conditions. When the stress is released, part of the core deformation is recovered instantly, which is an elastic deformation, while the other part of the deformation does not immediately reach the elastic deformation value, but has a relative hysteresis process. Such deformation is called non(-hysteresis) elastic recovery deformation. It is difficult to obtain in the in situ stress measurement, so people use nonelastic recovery deformation to carry out in situ stress measurement, that is, "anelastic strain recovery" method (ASR method).

3.1. Field Time-Effect Strain Monitoring. In this paper, the rock of Boshula tunnel of Sichuan-Tibet Railway is taken as the research object. The rock core is located at Borehole 2DSSZ-28, Boshula tunnel. Rock core depth is 714.4 m~715.3 (vertical hole); lithology is metamorphic sandstone.

Strain gauges are immediately affixed to the newly extracted core to measure the strain recovery of the core with time. A total of 3 strain gauges are attached at the same annular interval of 120° for each core, as shown in Figure 12. A0°, A45°, A90°, and A135° are strain gauges in four directions, respectively. A0° is axial strain gauge and A90° is circular strain gauge. The strain gauge should be

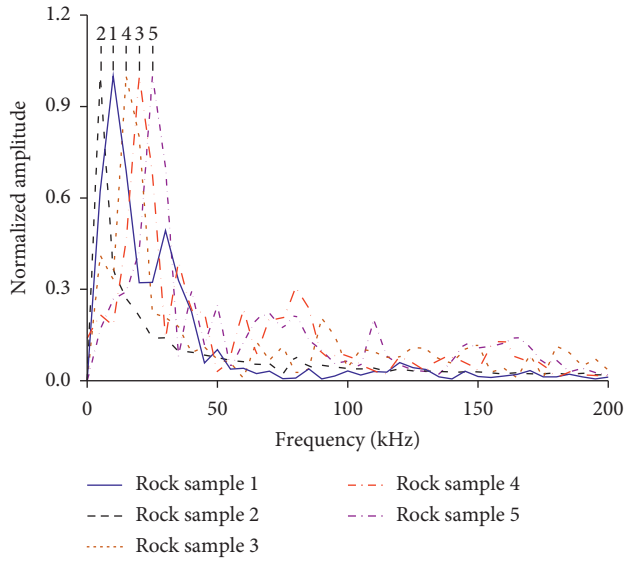

Figure 10: Amplitude–frequency characteristics of 5 granite sample CH1-CH3 region on the eve of failure.

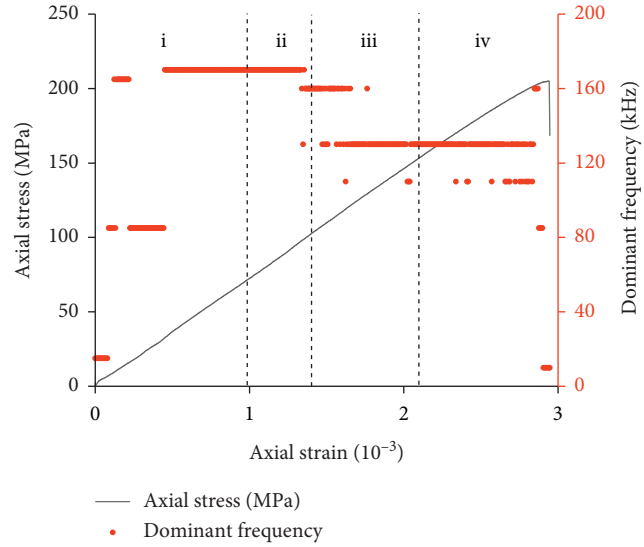

Figure 11: Dominant frequency variation of CH1-CH3 region in the uniaxial loading process of granite.

more than one diameter from both ends of the core to prevent end effect. The strain data acquisition interval was 10 min, and the anelastic change was stable until 96 h.

P-wave velocity were recorded at two points at an interval of 90° in the core annulus and then measured and recorded at the same measuring point every 12 hours, stable until 96 h.

The influence of temperature was removed from the strain recorded on-site, combined with the average wave velocity, as shown in Figure 13. Combined with Section 2.3, the ultrasonic wave velocity is basically stable in the elastic deformation process of the rock. But the continuous decrease of ultrasonic wave velocity appears in the time-effect deformation process of the rock on-site, indicating the existence of damage caused by the time-sensitive deformation process of the rock.

3.2. Rock Time-Effect Deformation Test. In order to further verify whether there is damage strain in the field time-effect strain, in situ stress was applied to the field rock sample through indoor test, compared with the springback values of axial strain in unloading on-site and indoor test.

The self-developed anelasticity load instrument, as shown in Figure 14, realizes the long-term uniaxial constant load test of rock samples. The rock samples retrieved from the site are processed into 64 × 128 mm samples that meet ISRM standards. The rock sample is installed on the anelasticity constant load instrument, and the time-effect strain data collector is used to collect the time-effect strain data of the rock sample. The strain collection interval of the test is 10 minutes. The measured value of in situ hydraulic fracturing in situ stress is 19.19 MPa, which is limited to the loading limit of the

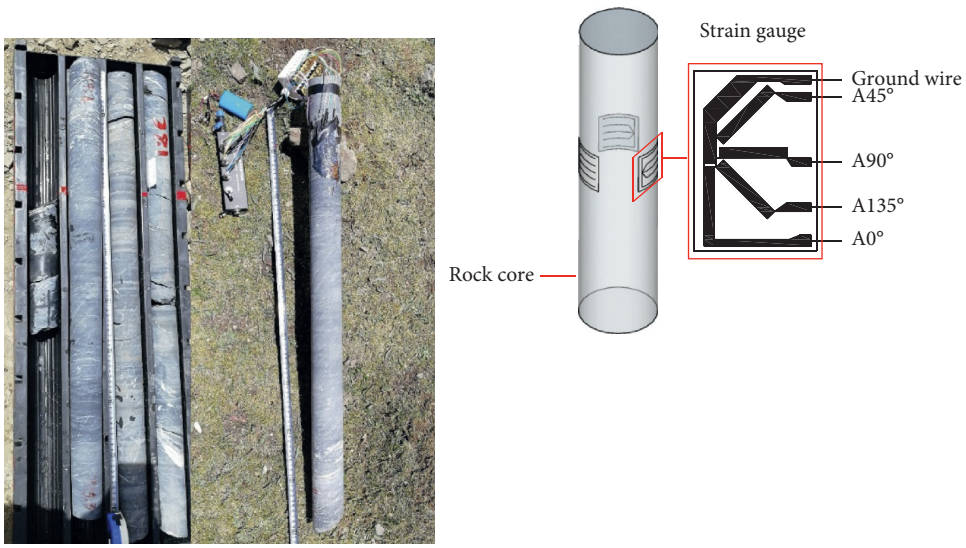

Figure 12: Arrangement of rock core strain gauge on-site.

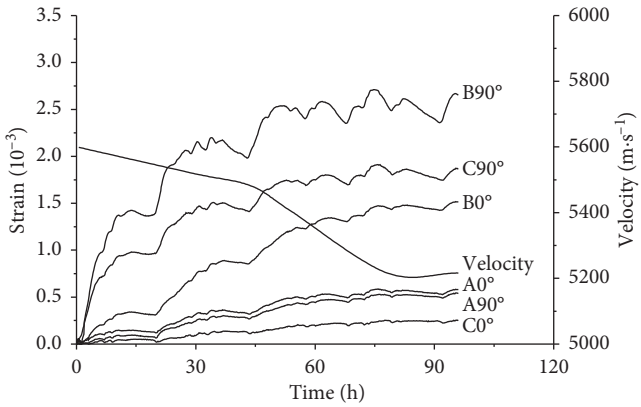

Figure 13: Field strain and ultrasonic wave velocity monitoring.

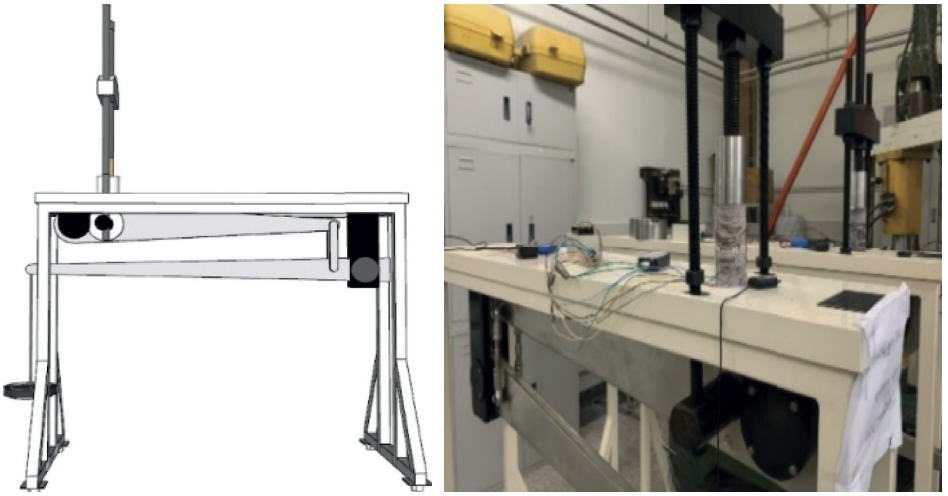

Figure 14: Rock time-effect loading equipment.

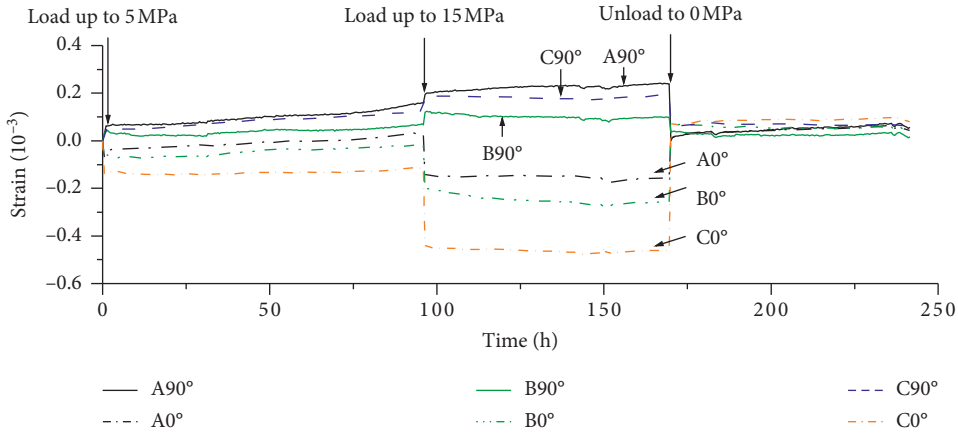

Figure 15: Time-effect strain under uniaxial loading and unloading of rock sample.

equipment. When loading in the design laboratory, first use 5 MPa constant load for 96 hours then increase the constant load pressure to 15 MPa and keep it for 72 hours. Unloading was carried out immediately after the experimental loading process was completed. After unloading, time-effect strain recovery data was collected for 72 hours.

Figure 15 shows the time-effect strain of the rock sample in the laboratory test. When it is loaded to 15 MPa, the average hoop strain was 176 $\mu\varepsilon$, and the average axial strain is 293 $\mu\varepsilon$. Compared with the strain in situ stress 19.19 MPa, the average hoop strain was 1702 $\mu\varepsilon$, axial strain on average was 783 $\mu\varepsilon$; with indoor test and field monitoring, the axial and hoop strain value order of magnitude, the difference is bigger; indoor test does not reproduce the time-effect deformation on-site, showing that there is damage deformation in unloading time-effect deformation. At the same time, the damage development is consistent with the continuous decrease of the wave velocity monitoring value, which proves that the ultrasonic wave velocity can monitor the damage evolution of the rock on-site.

4. Conclusions

In this paper, based on the dry-coupled point-contact ultrasonic monitoring system suitable for a variety of rock curvature, the stage transition characteristics and failure precursors of P-wave and S-wave at different positions of granite samples during uniaxial compression to failure were studied and verified by field engineering. The main conclusions are as follows:

(1) The P-wave velocity of CH1-CH2, CH1-CH4 and S-wave velocity of CH1-CH3 increased by 6.92%, 5.47%, and 4.04%, respectively, from the rock crack closure stage to the elastic stage, decreased by 5.17%, 10.37%, and 3.83%, respectively, from the stable crack growth stage to the unstable crack growth stage. The two waveforms showed obvious convertibility in the two stages transitions, and the velocity of the wave near the region of loading rose at a significantly higher rate than that of the rock as a whole; however, from the elastic stage to the stable crack growth stage, both the P-wave and S-wave velocities decreased by less than 3.6%, and the transition characteristics were not significant. The effectiveness of ultrasonic wave velocity in characterizing rock damage has been verified by in situ unloading time-effect deformation.

(2) The P-wave first arrived amplitude of CH1-CH2, CH1-CH4 and S-wave first arrived amplitude of CH1-CH3 increased by 104.2%, 58.6%, and 77.6%, respectively, from the rock crack closure stage to the elastic stage. From the elastic stage to the stable crack growth stage, the P-wave amplitude was flat, S-wave amplitude decreased by 16.2%, and then in the unstable crack growth stage, S-wave amplitude decreased by 39.1%, far higher than 18.4% and 5.6% of the P-wave of CH1-CH2 and CH1-CH4.

(3) The P-wave centroid frequency of CH1-CH2, CH1-CH4 and S-wave centroid frequency of CH1-CH3 increased by 8.6%, 12.1%, and 12.3%, respectively, from the rock crack closure stage to the elastic stage. But from the elastic stage to the stable crack growth stage, the variation was less than 1%, showing no significant change feature, but in the unstable crack growth stage, the three were of significant decline; S-wave was the most significant, with a drop of 25.4%. On the eve of failure, P-wave amplitude–frequency characteristics showed that the full-frequency amplitude decays rapidly.

(4) P-wave and S-wave velocity first arrived amplitude and centroid frequency of rock sample in crack closure stage, elastic stage and unstable crack growth stage showed significant change features, but from the elastic stage to the unstable crack growth stage, only S-wave dominant frequency shows obvious change features, reaching 6% decline, which is highly sensitive to the crack initiation. And on the eve of failure, S-wave amplitude-frequency characteristics are different from P-wave, showing the change feature from the state of multipeak in wide frequency to the state of single peak in low frequency; centroid frequency and amplitude–frequency characteristics

of S-wave have important practical significance for the identification of damage stage and failure prediction of rock based on ultrasonic monitoring.

Data Availability

The data used to support the findings of this study are included within the paper.

Conflicts of Interest

The authors declare that there are no conflicts of interest regarding the publication of this paper.

Acknowledgments

The study was supported by the National Key Research and Development Project of China (2018YFE0101100).

References

[1] W. Wuxing, G. Fengqiang, and Y. Weimin, "Experimental simulation study of spalling in deep rectangular tunnel with plastic fine grain marble," *Tunnelling and Underground Space Technology Incorporating Trenchless Technology Research*, vol. 98, Article ID 103319, 2020.

[2] M. S. Diederichs, "The 2003 canadian geotechnical colloquium: mechanistic interpretation and practical application of damage and spalling prediction criteria for deep tunnelling," *Canadian Geotechnical Journal*, vol. 44, no. 9, pp. 1082–1116, 2007.

[3] G. Fengqiang, S. Xuefeng, and L. Xibing, "Experimental investigation of strain rockburst in circular caverns under deep three-dimensional high-stress conditions," *Rock Mechanics and Rock Engineering*, vol. 52, no. 5, pp. 1459–1474, 2019.

[4] S. Guoshao, S. Yanjiong, and F. Xiating, "True-triaxial experimental study of the evolutionary features of the acoustic emissions and sounds of rockburst processes," *Rock Mechanics and Rock Engineering*, vol. 51, no. 2, pp. 375–389, 2018.

[5] Y. Peng, Z. Chen, and G. Qidong, "Acoustic wave test on mechanical properties variation of rocks under different damage degrees," *Rock and Soil Mechanics*, vol. 36, no. 12, pp. 3425–3432, 2015.

[6] G. Leucci and L. De Giorgi, "Experimental studies on the effects of fracture on the P and S wave velocity propagation in sedimentary rock ("Calcarenite del Salento")," *Engineering Geology*, vol. 84, no. 3-4, pp. 130–142, 2006.

[7] S. D. Goodfellow, M. Ghofranitabari, and M. B. Nasseri, "Evaluation of wave propagation properties during a true-triaxial rock fracture experiment using acoustic emission frequency characteristics," 2013.

[8] W. Jiong, Z. Wancheng, and G. Kai, "An acoustic emission data-driven model to simulate rock failure process," *Rock Mechanics and Rock Engineering*, vol. 53, no. 4, pp. 1605–1621, 2020.

[9] L. Jianpo, Z. Changyin, and S. Yingtao, "Temporal-spatial evolution of acoustic emission during progressive fracture processes around tunnel triggered by blast-induced disturbances under uniaxial and biaxial compression," *Tunnelling and Underground Space Technology*, vol. 96, Article ID 103229, 2020.

[10] W. GuiLin, Z. Liang, and W. Zhen, "Acoustic-mechanical responses of intact and flaw-contained rock deformation under uniaxial compression: a comparison," *Advances in Civil Engineering*, vol. 2019, Article ID 7940923, , 2019.

[11] T. Xiao, M. Huang, and M. Gao, "Experimental study of the mechanical characteristics of a rock-like material containing a preexisting fissure under loading and unloading triaxial compression," *Advances in Civil Engineering*, vol. 2020, Article ID 9374352, , 2020.

[12] Z. Dongxu, "Application of ultrasonic testing in rock test," *World Nonferrous Metals*, vol. 24, no. 4, pp. 233-234, 2017.

[13] W. Yu, L. Xiao, and H. Ruilin, "Review of research process and application of ultrasonic testing for rock and soil," *Journal of Engineering Geology*, vol. 23, no. 2, pp. 287–300, 2015.

[14] S. D. Falls and R. P. Young, "Acoustic emission and ultrasonic-velocity methods used to characterise the excavation disturbance associated with deep tunnels in hard rock," *Tectonophysics*, vol. 289, no. 1-3, pp. 1–15, 1998.

[15] Q. Dong, X. P. Li, and H. Zhao, "Experimental research on ultrasonic P-wave velocity variation of fractured rock mass under different stress paths," *Advanced Materials Research*, vol. 1069, pp. 35–39, 2014.

[16] Q. Shili, F. Xiating, and Z. Chuanqing, "Estimation of rockburst wall-rock velocity invoked by slab flexure sources in deep tunnels," *Canadian Geotechnical Journal*, vol. 51, no. 5, pp. 520–539, 2014.

[17] O. Uyanık, N. Sabbağ, and N. A. Uyanık, "Prediction of mechanical and physical properties of some sedimentary rocks from ultrasonic velocities," *Bulletin of Engineering Geology and the Environment*, vol. 78, no. 8, pp. 6003–6016, 2019.

[18] M. Heidari, R. Ajalloeian, A. Ghazifard, and M. Hashemi Isfahanian, "Evaluation of P and S wave velocities and their return energy of rock specimen at various lateral and axial stresses," *Geotechnical and Geological Engineering*, vol. 38, no. 3, pp. 3253–3270, 2020.

[19] M. J. S. Nascimento, J. J. S. D. Figueiredo, and C. B. D. Silva, "Analysis of Eshelby-Cheng's model in anisotropic porous cracked medium: an ultrasonic physical modeling approach," *Ultrasonics*, vol. 102, Article ID 106037, 2020.

[20] C. McCann and J. Sothcott, "Sonic to ultrasonic Q of sandstones and limestones: laboratory measurements at in situ pressures," *Geophysics*, vol. 74, no. 2, pp. WA93–WA101, 2009.

[21] L. Xinping, Z. Hang, and L. Yi, "Experimental study of propagation and attenuation of elastic wave in deep rock mass with joints," *Chinese Journal of Rock Mechanics and Engineering*, vol. 34, no. 11, pp. 2319–2326, 2015.

[22] T. Engelder and R. Plumb, "Changes in in situ ultrasonic properties of rock on strain relaxation," *International Journal of Rock Mechanics and Mining Sciences & Geomechanics Abstracts*, vol. 21, no. 2, pp. 75–82, 1984.

[23] J. Quan, C. Jie, and C. Jing, "Time-dependent damage investigation of rock mass in an in situ experimental tunnel," *Materials*, vol. 5, no. 8, pp. 1389–1403, 2012.

[24] J. Quan, C. Jie, and C. Jing, "The influence of pore structure in reservoir sandstone on dispersion properties of elastic waves," *Chinese Journal of Geophysics-Chinese Edition*, vol. 58, no. 9, pp. 3389–3400, 2015.

[25] S. Wenpeng, Y. Qinyong, and W. Huiming, "Experimental analysis of the influence of coupling methods on rock samples acoustic velocity measurement," *Progress in Geophysics*, vol. 33, no. 5, pp. 1951–1955, 2018.

[26] V. G. Shevaldykin and A. A. Samokrutov, "Ultrasonic low-frequency transducers with dry dot contact and their applications for evaluation of concrete structures," *International Ultrasonics Symposium*, vol. 1, pp. 793–798, 2002.

[27] L. Yang, L. Yuan, and Q. Lan, "Dry coupled ultrasonic testing technology and its application in testing rock dynamic and static parameters," *Journal of China Coal Society*, vol. 44, no. 5, pp. 1465–1472, 2019.

[28] F. B. Cegla, P. Cawley, J. Allin, and J. Davies, "High-temperature (>500°C) wall thickness monitoring using dry-coupled ultrasonic waveguide transducers," *IEEE Transactions on Ultrasonics, Ferroelectrics and Frequency Control*, vol. 58, no. 1, pp. 156–167, 2011.

[29] Y. Mingqing and S. Chengdong, "Measurement of S-wave velocity with probes for P-wave," *Chinese Journal of Rock Mechanics and Engineering*, vol. 11, no. 22, pp. 1841–1843, 2003.

[30] C. D. Martin and N. A. Chandler, "The progressive fracture of Lac du Bonnet granite," *International Journal of Rock Mechanics and Mining Sciences & Geomechanics Abstracts*, vol. 31, no. 6, pp. 643–659, 1994.

[31] L. Yuan, M. Xianghua, and L. Yang, "Dry coupled ultrasonic testing technology and automatic picking method determining arrival times," *Rock and Soil Mechanics*, vol. 41, no. 4, pp. 1455–1464, 2020.

[32] D. Shirole, A. Hedayat, and G. Walton, "Active ultrasonic monitoring of rocks under uniaxial compression," in *Proceedings of the American Rock Mechanics Symposium (ARMA)*, San Francisco, CA, USA, June 2017.